Carrier-Density-Induced Ferromagnetism in EuTiO_{3} Bulk and Heterostructures

Zhigang Gui and Anderson Janotti

Phys. Rev. Lett. **123**, 127201 — Published 17 September 2019

DOI: 10.1103/PhysRevLett.123.127201

Carrier density induced ferromagnetism in $EuTiO_3$ bulk and heterostructures

Zhigang Gui and Anderson Janotti
Department of Materials Science and Engineering,
University of Delaware, Newark, DE 19716, USA
(Dated: August 29, 2019)

$EuTiO_3$ is an antiferromagnetic material showing strong spin-lattice interactions, large magnetoelectric response, and quantum paraelectric behavior at low temperatures. Using electronic-structure calculations, we show that adding electrons to the conduction band leads to ferromagnetism. The transition from antiferromagnetism to ferromagnetism is predicted to occur at ∼0.08 electrons/Eu (∼1.4×10^{21} cm^{-3}). This effect is also predicted to occur in heterostructures such as $LaAlO_3/EuTiO_3$, where ferromagnetism is triggered by the formation of a high-density two-dimensional electron gas (2DEG) in the $EuTiO_3$. Our analysis indicates that the coupling between Ti $3d$ and Eu $5d$ plays a crucial role in lowering the Ti $3d$ conduction band in the FM phase, leading to an almost linear dependence of the energy difference between the FM and AFM ordering on the carrier concentration. These findings open up possibilities in designing field-effect transistors using $EuTiO_3$-based heterointerfaces to probe fundamental interactions between highly localized spins and itinerant, polarized charge carriers.

The coupling between spin, lattice, and charge in complex oxides gives rise to extremely rich phase diagrams including magnetism, ferroelectricity, magnetoelectricity, superconductivity, and colossal magnetoresistance[1, 2]. The combination of these three degrees of freedom is found in rare-earth titanates where itinerant Ti $3d$ electrons couple with localized rare-earth $4f$ electrons, in the presence of TiO_6 octahedral tilt and rotations [3]. Advances in epitaxial growth of oxide-based heterostructures, with meticulous control of thickness down to a monatomic layer, have enabled the study of the cross coupling of these interactions. Recently, an electric-field-tunable spin-polarized and superconducting quasi-2D electron system was created by inserting a few unit-cell thick layer of $EuTiO_3$ at the $LaAlO_3/SrTiO_3$ interface [4]. The $LaAlO_3/EuTiO_3/SrTiO_3$ δ-doped heterostruture was found to display different ground states depending on the carrier density, from Kondo-like transport at low carrier concentrations, to superconductivity and itinerant ferromagnetism as the 2D carrier density increases, with an intriguing transition from ferromagnetic to superconducting as a function of temperature. It is unclear whether a 2D superconducting state with unconventional order parameter is established as a result of the spin polarization of the itinerant Ti $3d$ electrons, or ferromagnetism and superconductivity coexist but at different depths inside the quasi-2D electron system [4]. Unraveling the interactions between the itinerant Ti-$3d$ and the localized Eu-$4f$ electrons is key to understanding these observations.

Electronic structure calculations are employed to investigate how excess electrons in the bulk of $EuTiO_3$ and at the $LaAlO_3/EuTiO_3$ interface affect the ordering of the Eu-$4f$ spins. As shown in Figure 1, we find that a transition from G-type antiferromagnetic (AFM) to ferromagnetic (FM) ordering occurs as the carrier concentration increases. The fundamental interactions underlaying

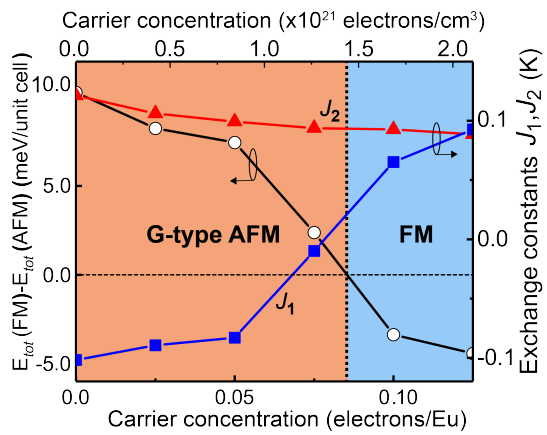

FIG. 1. Total-energy difference between the FM and G-AFM orderings, and first and second nearest-neighbor exchange constants, J_1 and J_2, as a function of carrier concentration in $EuTiO_3$.

,

the FM ordering are explained in terms of orbital couplings. We also show that the 2DEG in $EuTiO_3/LaAlO_3$ heterostructures also makes the $EuTiO_3$ ferromagnetic, which we attribute to the favored band alignment and charge transfer accross the LaO-TiO_2 interface.

Our calculations are based on the density functional theory (DFT) [5, 6] and the HSE06 hybrid functional [7, 8] as implemented in the VASP code [9]. We use projected augmented wave potentials [10] with plane-wave basis set with a cutoff of 550 eV. For integrations over the Brillouin zone, we use a $7\times7\times5$ k-point mesh for bulk 20-atom cells and $3\times3\times1$ for the $EuTiO_3/LaAlO_3$ superlattices (composed of 7 unit-cell thick $EuTiO_3$ and 3 unit-cell thick $LaAlO_3$). The atomic positions are fully relaxed until the forces on each atom are less than 0.005 eV/Å and total-energy differences between consecutive steps

are less than 10^{-6} eV. In the bulk calculations of the FM and AFM orderings, the lattice parameters and atomic positions are fully relaxed. For the $EuTiO_3/LaAlO_3$ superlattices, the in-plane lattice parameters were kept fixed during the structural relaxation to mimic the epitaxial growth on a $SrTiO_3$ substrate. Testing calculations based on DFT+U [11–13] demonstrate robustness of our results and conclusions (Supplemental Material [14]).

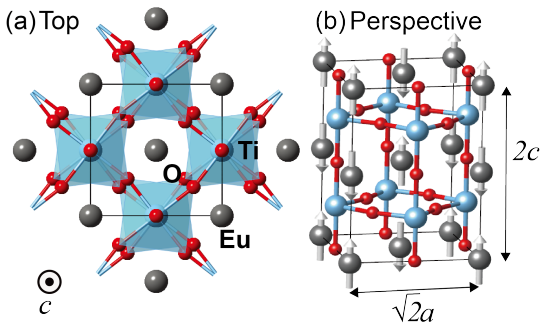

FIG. 2. Ball & stick model of the 20-atom unit cell of $EuTiO_3$ seen (a) from the [001] direction with anti-phase rotations of oxygen octahedra around the c axis; (b) perspective view of the G-AFM ordering.

$EuTiO_3$ has a perovskite crystal structure with lattice parameters very close to those of $SrTiO_3$. In contrast to $SrTiO_3$, $EuTiO_3$ is magnetic, with a high spin $S = 7/2$ per Eu ($4f^7$). At temperatures lower than 5 K, $EuTiO_3$ displays G-type AFM ordering [15–17]. Above 5 K, $EuTiO_3$ becomes paramagnetic. DFT calculations and experiments have demonstrated that epitaxial $EuTiO_3$ thin films show FM ordering under tensile strain [13, 18–21], opening the door to higher-temperature implementations of strong ferromagnetic ferroelectrics and, potentially, to various device applications such as magnetic sensors, high-density multistate memory elements, tunable microwave filters, phase shifters and resonators. The use of epitaxial strain to stabilize the FM ordering has its limitations, relying on the speed of lattice response for switching between FM and AFM. Here, instead, we turn to doping as a way of controlling the magnetic ordering, i.e., we investigate how charge carriers affect the ordering of the Eu spin moments. Changing the doping level through a gated structure would allow for controlling the magnetization and exploring the fundamental interactions between itinerant electrons and highly localized spin moments.

For studying the effects of charge carriers in $EuTiO_3$, we added electrons to the perfect bulk represented by a unit cell containing 20 atoms, which allows for the description of both FM and G-type AFM orderings, including the effects of octahedral tilt and rotations. The excess electrons are compensated by a homogeneous neutralizing background to ensure the system is charge neutral. We chose to add electrons to the conduction band, instead of explicitly adding shallow-donor impurities, to separate the effects of excess charge carriers from the chemical or size effects of the impurities. Possible ways of doping, such as incorporation of impurities and through polar/non-polar interfaces in heterostructures are discussed.

The spin configuration of the G-type AFM ordering in $EuTiO_3$ is shown in Figure 2. In both AFM and FM $EuTiO_3$ there is a small anti-phase octahedral rotation around the c axis. The calculated lattice parameters for the G-type AFM ground state are $a = 3.888$ Å, $c = 3.924$ Å, and $\alpha = 7.24°$, in good agreement with the experimental values $a = 3.903$ Å, $c = 3.908$ Å, and $\alpha = 3.03°$ [22, 23]. The lattice parameters for the FM ordering are $a = 3.888$ Å, $c = 3.926$ Å, and $\alpha = 7.23°$, i.e., very close to those of the AFM ground state. Doping within the range considered in the present work, i.e., up to 0.125 electrons/Eu, leads to negligible changes in lattice parameters, of less than 0.68%.

To understand the effects of carriers on the magnetic ordering, we first analyze the electronic structure of undoped $EuTiO_3$. The band structure of the G-AFM and FM orderings are shown in Figure 3. The AFM and FM configurations display a band gap, which is slightly smaller in the FM than in the AFM, and in both cases we find a magnetic moment of $S = 7/2$/Eu. The gap separates the occupied narrow Eu-4f band from the unoccupied conduction band derived mostly from Ti-3d orbitals. The O-2p band is about 2 eV below the occupied Eu-4f band. These results are in good agreement with previous HSE06 calculations and photoemission measurements [20], as well as diffusive reflectance [17] and absorption [24, 25] spectra. We also find a significant contribution from Eu 5d to the lowest-energy conduction bands, which suggests a coupling with Ti 3d, as seen in the orbital-projected density of states in Figure 4. For the undoped case, we find the G-AFM to be lower in energy than the FM ordering by 10.3 meV per unit cell, consistent with previous studies [13, 15–21]. It is noteworthy that the conduction-band minimum (CBM) of the FM phase is lower than that of the AFM, i.e., ΔE_{CBM}=-0.10 eV. which we determine following Ref. [26]

By inspecting the band structures in Figure 3, we note that the excess electrons will be occupying the Ti 3d conduction band. We also note that the exchange splitting at the CBM gives a net polarization to the excess electrons, which is aligned with the FM ordering of the Eu spins. As electrons are added to $EuTiO_3$, the total-energy difference between the FM and AFM phases [$\Delta E_{\mathrm{FM-AFM}}$=$E_{tot}$(FM) − $\mathrm{E_{tot}}$(AFM)] decreases (Figure 1). When the added electron concentration exceeds 0.08 electrons/Eu (1.4×10^{21} electrons/cm^3), the FM becomes more energetically favorable than the AFM ordering ($\Delta E_{\mathrm{FM-AFM}} < 0$). The monotonic decrease of ΔE_{FM-AFM} with the excess carriers and the nega-

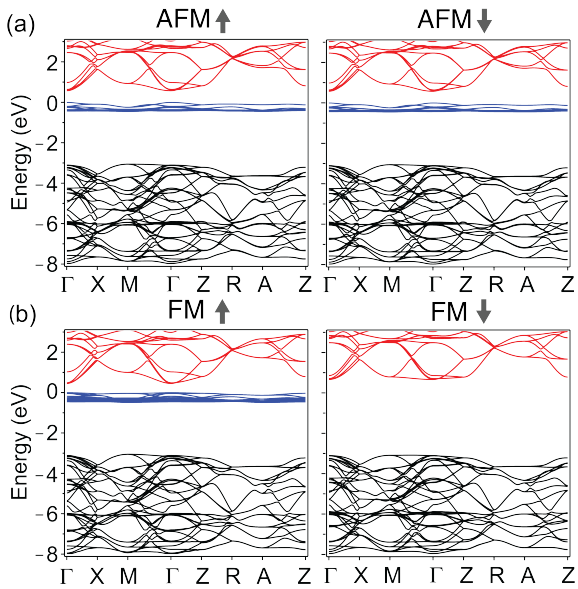

FIG. 3. Electronic band structures of $EuTiO_3$ for (a) G-type antiferromagnetic (AFM) ordering, and (b) ferromagnetic (FM) ordering. The zero in the energy axis was set to top of the occupied Eu-4f band.

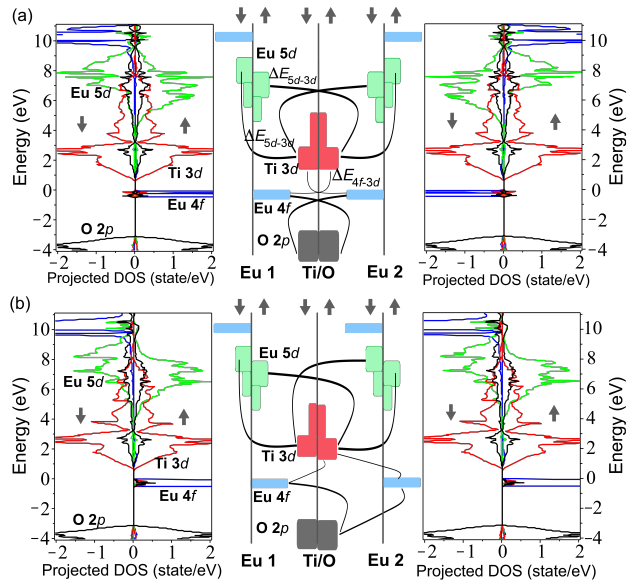

FIG. 4. Density of states projected on Eu-4f orbitals (blue), Eu-5d orbitals (green), Ti-3d orbitals (red), and O -2p orbitals (black), and the derived inter-band coupling diagrams for the (a) G-type antiferromagentic (AFM) and (b) ferromagnetic (FM) ordering of undoped $EuTiO_3$. In the inter-band coupling diagrams, the solid curvy arrows indicate the most relevant couplings. The exchange splitting in the O-2p bands and Ti-3d bands are enlarged for ease of representation. The zero in the energy axis was set to the maximum of the occupied Eu-4f band.

tive sign of ΔE_{CBM} suggest a simple rigid-band filling model: as electrons are added to the conduction band, the FM ordering will become more stable than the AFM when $n \times |\Delta E_{CBM}| > \Delta E_{FM-AFM}$, where n is the carrier concentration. From this simple picture, the estimated electron concentration that would make the FM more stable amounts to $n = 0.03$ electrons/Eu, in reasonable agreement with the direct calculated value of $n = 0.08$ electrons/Eu shown in Figure 1. A comparison of the electronic band structures of the undoped and doped $EuTiO_3$ (see Supplemental Material [14]) shows that the bands remain intact upon doping, corroborating the rigid-band filling picture.

Why is the CBM in the FM phase lower than that in AFM in $EuTiO_3$, i.e., $\Delta E_{CBM} < 0$? We explain it based on the coupling between the Ti-3d (t_{2g}) and the Eu-5d (t_{2g}), Eu-4f, and O-2p bands, of which the Eu 5d-Ti 3d and Eu 4f-Ti 3d are the most relevant because they act differently in the case of the AFM and FM orderings. From the orbital-projected DOS, we constructed the inter-band interaction diagrams shown in Figure 4, where we highlight the relevant couplings that affect the position of the Ti-3d band. The energy shift of the Ti-3d band due these couplings is denoted as $\Delta E^X_{5d-3d}(\uparrow;1,2)$, $\Delta E^X_{5d-3d}(\downarrow;1,2)$, $\Delta E^X_{4f-3d}(\uparrow;1,2)$, $\Delta E^X_{4f-3d}(\downarrow;1,2)$, where $\uparrow$ or $\downarrow$ indicate the spin channel, X refers to the AFM or FM ordering, and 1 or 2 represents the index of the two nearest Eu atoms to a given Ti atom. Thus, the spin-up Ti-3d band of the AFM ordering is shifted according to:

$$\Delta^{AFM} = \Delta E^{AFM}_{4f-3d}(\uparrow;1) - \Delta E^{AFM}_{5d-3d}(\uparrow;1) - \Delta E^{AFM}_{5d-3d}(\uparrow;2), \quad (1)$$

where we neglected $\Delta E^{AFM}_{4f-3d}(\uparrow;2)$ due to the large energy separation between the Ti-3d band and the empty Eu-4f band, and the small overlap of the Ti-3d and Eu-4f orbitals due to the large distance between the Ti and Eu atoms. An equivalent expression can be written for the spin-down Ti-3d band.

For the FM ordering, the spin-up Ti-3d band is shifted according to:

$$\Delta^{FM} = \Delta E^{FM}_{4f-3d}(\uparrow;1) + \Delta E^{FM}_{4f-3d}(\uparrow;2) - \Delta E^{FM}_{5d-3d}(\uparrow;1) - \Delta E^{FM}_{5d-3d}(\uparrow;2). \quad (2)$$

We note that $E^{FM}_{5d-3d}(\uparrow;1) = E^{FM}_{5d-3d}(\uparrow;2) \approx \Delta E^{AFM}_{5d-3d}(\uparrow;1) \gg \Delta E^{AFM}_{5d-3d}(\uparrow;2)$. Based on the DOS shown in Figure 4, and Eqs. 1 and 2, we conclude that the Eu 5d-Ti 3d coupling is responsible for lowering the Ti-3d band in the FM compared to that in the AFM ordering.

In the case of undoped $EuTiO_3$, it has been proposed that the competition between the antiferromagnetic superexchange and an indirect ferromagnetic exchange via

the Eu 5d states leads to a delicate balance between the AFM and FM phases [20]. Here we show how this competition between the AFM and FM orderings is altered by the presence of electrons in the Ti-3d conduction band. Basically, adding electrons to the conduction band favors the FM phase because its CBM is lower than that in the AFM phase.

It could also be argued that the stabilization of the FM ordering upon doping in $EuTiO_3$ follows the Stoner model [27]. As the doping concentration in the Ti-3d t_{2g} bands increases, the density of states at the Fermi level increases; at a certain doping concentration, the spin splitting of the Ti-3d bands becomes energetically favorable (since it reduces the electron-electron repulsion), which is consistent with the Stoner picture of magnetism [27]. However, it is important to note that the spin splitting of the Ti-3d bands is already present in the FM undoped $EuTiO_3$. The polarized Eu-4f bands lead to the spin polarization of the Eu-5d bands, which are composed of orbitals that are quite delocalized in space and overlap with Ti-3d orbitals, thus leading to a spin-split conduction band. In the rigid-band filling model, adding electrons then lowers the energy of the FM with respect the AFM ordering.

How can electrons be added to the conduction band of $EuTiO_3$ and how to control their concentration? A conventional method of adding electrons to the conduction band of a semiconductor is to incorporate shallow-donor impurities. These are atoms that typically sit to the right of the host atoms in the periodic table. For $EuTiO_3$, there are a few possibilities: trivalent impurities sitting on the Eu site, such as Gd and La, pentavalent impurities sitting on the Ti site, such as Nb, or F siting on the O site. In addition, one could incorporate H, either as interstitial bonded to O, or substitutional replacing O atoms. Both forms have been reported to act as shallow donors in many oxides [28, 29].

Experimentally, it has been found that $EuTiO_3$ doped with either La, Gd, Dy, Nb, or H leads to ferromagnetism [30–34]. It has also been reported that by controlling oxygen partial pressure leads to conducting ferromagnetic films [35]. Specifically, $EuTiO_{3-x}H_x$, with x as low as 0.07, leads to ferromagnetic powders and thin films [34], and that ferromagnetism is observed in $EuTi_{1-x}Nb_xO_3$ for $x \geq 0.1$ [33]. These results are in good agreement with our predicted AFM-FM transition at ∼0.08 electrons/Eu. In all these reports, the emergence of ferromagnetism in doped $EuTiO_3$ has been attributed to the Ruderman-Kittel-Kasuya-Yosida (RKKY) interaction, yet without any further justification. RKKY is often used to explain the exchange interaction between itinerant electrons and localized magnetic moments. Here, we find that the interaction between the Ti 3d and Eu 4f is of secondary importance, and that the Eu 5d-Ti 3d coupling (Figure 4) is key to stabilizing the FM ordering with increasing carrier concentration.

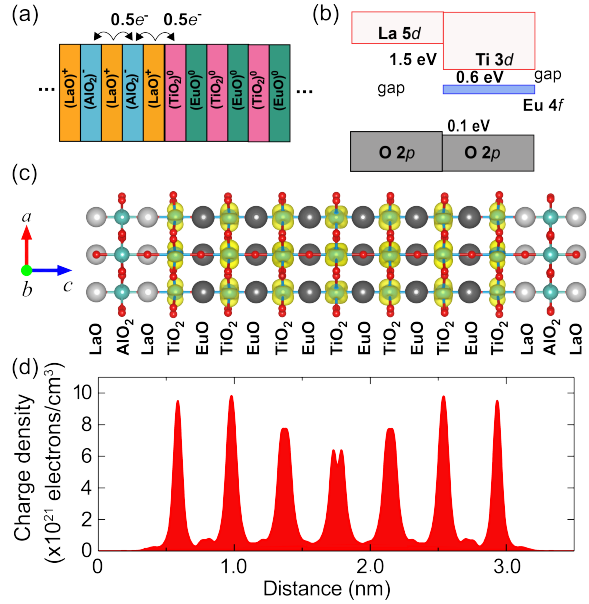

FIG. 5. (a) Formation of a 2DEG at the $LaAlO_3/EuTiO_3(001)$ interface with a LaO-TiO_2 termination. (b) Band alignment at the $LaAlO_3/EuTiO_3$. (c) Distribution of the charge carriers in the $LaAlO_3/EuTiO_3(001)$ superlattice with two equivalent LaO-TiO_2 interfaces, with isosurface set to 20% of the maximum value. (d) Planar-averaged excess charge as a function of the distance along the c axis of the superlattice in (c), showing excess charge accumulation in the $EuTiO_3$.

We can also add conduction electrons to $EuTiO_3$ though a heterointerface. In analogy to $LaAlO_3/SrTiO_3(001)$ [36–40], or $GdTiO_3/SrTiO3(001)$[41], we predict that a 2DEG will form at the $LaAlO_3/EuTiO_3$ with LaO-TiO_2 termination. In such systems, the charge transfer to the $EuTiO_3$ layer occurs due to the valence mismatch and the band alignment at the interface [38–40]. The conduction band in the band insulator $LaAlO_3$ or in the Mott insulator $GdTiO_3$ lie higher in energy than the conduction band in $EuTiO_3$ such that, at the LaO-TiO_2 termination the excess electrons from the LaO donor layer is accommodated in the conduction band of $EuTiO_3$ [26].

Basically, $LaAlO_3$ can be thought as composed of alternating charged planes $(LaO)^+$ and $(AlO_2)^-$ along the [001] direction, whereas $EuTiO_3$ is composed of charge-neutral planes $(EuO)^0$ and $(TiO_2)^0$. In the $LaAlO_3$, each $(LaO)^+$ gives $0.5e^-$ per unit-cell area to the right and $0.5e^-$ to the left $(AlO_2)^-$, as indicated in Figure 5(a). Thus, at the LaO-TiO_2 interface, there will be an excess of $0.5e^-$ per unit-cell area, which due to the conduction-band offset, is accommodated on the $EuTiO_3$ side, forming a 2DEG near the interface. The excess electrons from the 2DEG is sufficient to turn the $EuTiO_3$ layer ferromagnetic.

To demonstrate this effect, we first calculated the band alignment between $LaAlO_3$ and $EuTiO_3$, following the procedure described in [26]; the result is shown in Figure 5(b). Then we performed calculations for an $LaAlO_3/EuTiO_3(001)$ superlattice with two equivalent LaO-TiO_2 interfaces. The structure of the superlattice $LaAlO_3/EuTiO_3$ is given in Figure 5(c). The distribution of the excess charges in the $EuTiO_3$ layer is also shown in Figure 5(c) and the planar-averaged excess charge density along the c axis is shown in Figure 5(d).

We find that the FM is lower than the AFM ordering by 9.7 meV/(unit cell) in the heterostructure, and that each Eu atom in the heterostructure holds a magnetic spin moment of $S = 7/2$/Eu ($4f^7$). Considering the thickness of the $EuTiO_3$ layer (23.5 Å), we obtain an excess electron concentration of 2.4×10^{21} e^-/cm^3 since each interface gives 0.5 electron per unit cell area. The stability of the FM ordering is thus explained by the presence of the excess electrons in the conduction band of $EuTiO_3$, consistent with the results for bulk shown in Figure 1. The excess electrons are uniformly distributed over the Ti-3d orbitals in $EuTiO_3$, contributing with negligibly small moments to the total spin. Our results also explain the observed ferromagnetism in the $LaAlO_3/EuTiO_3/SrTiO_3$ δ-doped heterostrutures [4], which arises from the charge transfer through the $LaAlO_3/EuTiO_3$ interface.

The results for the $LaAlO_3/EuTiO_3(001)$ in Figure 5 suggest that the ferromagnetism in the $EuTiO_3$-based heterostructures could be controlled by an electric field. In a field-effect transistor design, and at low temperatures, an electric field applied through a gate electrode could be used to deplete/accumulate charge carriers in the $EuTiO_3$ layer near the interface, inducing FM/AFM transitions, thus enabling the control of the magnetic ordering through a gate voltage. Such FET has already been demonstrated in the case of $LaAlO_3/SrTiO_3$ [37, 42] and $GdTiO_3/SrTiO_3$ [43], although a complete depletion of the excess charge in the $SrTiO_3$ layer has been proved challenging. Such device could be used to manipulate and control the magnetic ordering in $EuTiO_3$ thin films, and also to investigate the fundamental interactions between the electrons in the 2DEG with the large Eu spin moments near the interface through the current between source and drain.

ACKNOWLEGMENTS

This work was funded by the NSF Early Career Award grant number DMR-1652994. We used the computing resources provided by the Extreme Science and Engineering Discovery Environment (XSEDE), supported by National Science Foundation grant number ACI-1053575, and the high-performance computing resources at the University of Delaware.

[1] H. Y. Hwang, Y. Iwasa, M. Kawasaki, B. Keimer, N. Nagaosa, and Y. Tokura, Nat. Mater. **11**, 103 (2012).
[2] W. Eerenstein, N. D. Mathur, and J. F. Scott, Nature **442**, 759 (2006).
[3] J. B. Goodenough and J.-S. Zhou, *Localized to Itinerant Electronic Transition in Perovskite Oxides*, Vol. 98 (Springer, Berlin, Heidelberg, 2001) pp. 17–113.
[4] D. Stornaiuolo, C. Cantoni, G. M. De Luca, R. Di Capua, E. Di. Gennaro, G. Ghiringhelli, B. Jouault, D. Marrè, D. Massarotti, F. Miletto Granozio, I. Pallecchi, C. Piamonteze, S. Rusponi, F. Tafuri, and M. Salluzzo, Nat. Mater. **15**, 278 (2015).
[5] P. Hohenberg and W. Kohn, Phys. Rev. **136**, B864 (1964).
[6] W. Kohn and L. J. Sham, Phys. Rev. **140**, A1133 (1965).
[7] J. Heyd, G. E. Scuseria, and M. Ernzerhof, J. Chem. Phys. **118**, 8207 (2003).
[8] A. V. Krukau, O. A. Vydrov, A. F. Izmaylov, and G. E. Scuseria, J. Chem. Phys. **125**, 224106 (2006).
[9] G. Kresse and J. Furthmüller, Phys. Rev. B **54**, 11169 (1996).
[10] P. E. Blöchl, Phys. Rev. B **50**, 17953 (1994).
[11] J. P. Perdew, A. Ruzsinszky, G. I. Csonka, O. A. Vydrov, G. E. Scuseria, L. A. Constantin, X. Zhou, and K. Burke, Phys. Rev. Lett. **100**, 136406 (2008).
[12] V. I. Anisimov, F. Aryasetiawan, and A. I. Lichtenstein, J. Phys.: Cond. Matter **9**, 767 (1997).
[13] Y. Yang, W. Ren, D. Wang, and L. Bellaiche, Phys. Rev. Lett. **109**, 267602 (2012).
[14] See Supplemental Material [url] for details on the DFT+U calculations, band structures and projected DOS of $EuTiO_3$ for the G-type AFM and FM orderings (with and without doping), the variation of the lattice parameters with doping concentration, and the determination of the exchange constants J_1 and J_2.
[15] T. R. McGuire, M. W. Shafer, R. J. Joenk, H. A. Alperin, and S. J. Pickart, J. Appl. Phys. **37**, 981 (1966).
[16] C.-L. Chien, S. DeBenedetti, and F. D. S. Barros, Phys. Rev. B **10**, 3913 (1974).
[17] H. Akamatsu, K. Fujita, H. Hayashi, T. Kawamoto, Y. Kumagai, Y. Zong, K. Iwata, F. Oba, I. Tanaka, and K. Tanaka, Inorg. Chem. **51**, 4560 (2012).
[18] C. J. Fennie and K. M. Rabe, Phys. Rev. Lett. **97**, 267602 (2006).
[19] J. H. Lee, L. Fang, E. Vlahos, X. Ke, Y. W. Jung, L. F. Kourkoutis, J.-W. Kim, P. J. Ryan, T. Heeg, M. Roeckerath, V. Goian, M. Bernhagen, R. Uecker, P. C. Hammel, K. M. Rabe, S. Kamba, J. Schubert, J. W. Freeland, D. A. Muller, C. J. Fennie, P. Schiffer, V. Gopalan, E. Johnston-Halperin, and D. G. Schlom, Nature **466**, 954 (2010).
[20] H. Akamatsu, Y. Kumagai, F. Oba, K. Fujita, H. Murakami, K. Tanaka, and I. Tanaka, Phys. Rev. B **83**, 214421 (2011).
[21] K. Tanaka, K. Fujita, Y. Maruyama, Y. Kususe, H. Murakami, H. Akamatsu, Y. Zong, and S. Murai, J. Mater. Res. **28**, 1031 (2013).
[22] T. Katsufuji and H. Takagi, Phys. Rev. B **64**, 054415 (2001).
[23] J. Köhler, R. Dinnebier, and A. Bussmann-Holder, Phase Transitions **85**, 949 (2012).

[24] J. H. Lee, X. Ke, N. J. Podraza, L. F. Kourkoutis, T. Heeg, M. Roeckerath, J. W. Freeland, C. J. Fennie, J. Schubert, D. A. Muller, P. Schiffer, and D. G. Schlom, Appl. Phys. Lett. **94**, 2009 (2009).

[25] T. Kolodiazhnyi, M. Valant, J. R. Williams, M. Bugnet, G. A. Botton, N. Ohashi, and Y. Sakka, J. Appl. Phys. **112**, 083719 (2012).

[26] L. Bjaalie, B. Himmetoglu, L. Weston, A. Janotti, and C. G. Van de Walle, New J. Phys. **16**, 025005 (2014).

[27] E. C. Stoner, Proc. R. Soc. London, Ser. A **169**, 339 (1939).

[28] C. G. Van de Walle, Phys. Rev. Lett. **85**, 1012 (2000).

[29] A. Janotti and C. G. Van de Walle, Nat. Mater. **6**, 44 (2007).

[30] T. Katsufuji and Y. Tokura, Phys. Rev. B **60**, R15021 (1999).

[31] K. Yoshii, M. Mizumaki, A. Nakamura, and H. Abe, J. Sol. Stat. Chem. **171**, 345 (2003).

[32] Y. Kususe, H. Murakami, K. Fujita, I. Kakeya, M. Suzuki, S. Murai, and K. Tanaka, Jap. J. Appl. Phys. **53**, 05FJ07 (2014).

[33] L. Li, J. R. Morris, M. R. Koehler, Z. Dun, H. Zhou, J. Yan, D. Mandrus, and V. Keppens, Phys. Rev. B **92**, 024109 (2015).

[34] T. Yamamoto, R. Yoshii, G. Bouilly, Y. Kobayashi, K. Fujita, Y. Kususe, Y. Matsushita, K. Tanaka, and H. Kageyama, Inorganic Chemistry **54**, 1501 (2015).

[35] K. Kugimiya, K. Fujita, K. Tanaka, and K. Hirao, J. Mag. and Mag. Mater. **310**, 2268 (2007).

[36] A. Ohtomo and H. Y. Hwang, Nature **427**, 423 (2004).

[37] S. Thiel, G. Hammerl, A. Schmehl, C. W. Schneider, and J. Mannhart, Science **313**, 1942 (2006).

[38] J. Lee and A. A. Demkov, Phys. Rev. B **78**, 193104 (2008).

[39] R. Pentcheva and W. E. Pickett, Phys. Rev. B **74**, 035112 (2006).

[40] A. Janotti, L. Bjaalie, L. Gordon, and C. G. Van de Walle, Phys. Rev. B **86**, 241108 (2012).

[41] P. Moetakef, T. A. Cain, D. G. Ouellette, J. Y. Zhang, D. O. Klenov, A. Janotti, C. G. Van de Walle, S. Rajan. S. James Allen and S. Stemmer, Appl. Phys. Lett. **99**, 232116 (2011).

[42] B. Förg, C. Richter, and J. Mannhart, Appl. Phys. Lett. **100**, 053506 (2012).

[43] M. Boucherit, O. Shoron, C. A. Jackson, T. A. Cain, M. L. C. Buffon, C. Polchinski, S. Stemmer, and S. Rajan, Appl. Phys. Lett. **104**, 182904 (2014).